Sixfold degenerate nodal-point phonons: Symmetry analysis and materials realization

Chengwu Xie,[1,*] Ying Liu,[2,*] Zeying Zhang,[3,†] Feng Zhou,[1] Tie Yang,[1] Minquan Kuang,[1] Xiaotian Wang,[1,‡] and Gang Zhang[4,§]

[1]*School of Physical Science and Technology, Southwest University, Chongqing 400715, China*
[2]*School of Materials Science and Engineering, Hebei University of Technology, Tianjin 300130, China*
[3]*College of Mathematics and Physics, Beijing University of Chemical Technology, Beijing 100029, China*
[4]*Institute of High Performance Computing, Agency for Science, Technology and Research (A*STAR), 138632 Singapore*

(Received 26 April 2021; revised 20 June 2021; accepted 16 July 2021; published 28 July 2021)

Multifold degenerate fermions in electronic structures of topological materials give rise to many interesting physics properties. Among them, three-, six-, and eightfold degenerate fermions in condensed matter systems are considered important because these fermions are not allowed in high-energy physics due to restriction posed by Poincáre symmetry. Phonons are the basic emergent boson of the crystalline lattice. Moreover, topological phonons also exist in crystalline solids, like fermionic electrons, due to the crystal symmetry constraints. Two-, three-, and fourfold degenerate phonons were predicted previously. This study proposes degenerate phonons with the maximum fold, i.e., sixfold; we find them in five space groups (with numbers 218, 220, 222, 223, and 230) through a detailed symmetry analysis. We also propose a series of realistic materials with above-mentioned space group numbers that host sixfold degenerate nodal-point phonons at the high-symmetry points H (or R) point using first-principles calculations. Finally, as examples, we investigate the surface phonon spectrum of C_3N_4, Sc_4C_3, Y_4Sb_3, and K_8Si_{46} materials and find two obvious projected phonon surface states on (110) or (100) surfaces.

DOI: 10.1103/PhysRevB.104.045148

I. INTRODUCTION

Beyond the fundamental fermions—Weyl, Dirac, and Majorana—three-, six-, and eightfold degenerate fermions [1–6] are allowed in condensed matter systems due to fewer constraints placed by the space group (SG) symmetries. A symmetry-protected crossing of three, six, and eight bands appear around the Fermi level (E_F) in three-, six-, and eightfold degenerate nodal-point materials, respectively, leading to exotic fermionic excitations.

Three-, six-, and eightfold degenerate nodal-point semimetals generally belong to symmetry-enforced semimetals [2]. Because they basically depend on constraints derived from SG symmetry, possibly combined with time-reversal symmetry $\mathcal{T}$. Threefold degenerate nodal-point semimetals were first predicted in tungsten carbide (WC) types of AB materials (A = Zr, Nb, Mo, Ta, W; B = C, N, P, S, Te) [4,7,8] using first-principles calculations and symmetry analysis. A series of materials, including strained HgTe [4], half-Heusler alloys [9], and trigonal layered $PtBi_2$ [10], have been subsequently reported to host triple-point band crossings. Importantly, the triple-point fermions were confirmed in MoP and WC [11,12] in the experiment using angle-resolved photoemission measurements. Moreover, Wieder *et al.* [13] proposed an eightfold degenerate (named double-Dirac) nodal point based on the symmetry analysis. Especially, they stated that the A point in $P4/ncc$ (No. 130) and $P4_2/mbc$ (No. 135) SGs must be eightfold degenerate. Thereafter, Bradlyn *et al.* [5] proposed materials $CuBi_2O_4$, $PdBi_2O_4$, PdS, and CsSn with No. 130 and No. 135 SGs containing eightfold fermions at A point. Also, they proposed that Ta_3Sb, $LaPd_3S_4$, and Nb_3Bi with No. 223 SG host eightfold fermions at R point. Furthermore, Zhang *et al.* [14] in 2020 predicted eightfold fermionic excitations in high-quality $TaTe_4$ single crystals. Sixfold fermions were proposed in [Al/Mg]Pt, CoGe, $KMgBO_4$ [15,16] with $P2_13$ (No. 198) SG, Li_2Pd_3B [17,18] with $P4_332$ (No. 212) SG, $PdSb_2$ [19–21] with $Pa\bar{3}$ (No. 205) SG, and $Li_{12}Mg_3Si_4$ [22] and Re_2C_3 [23] with $I\bar{4}3d$ (No. 220) SG. However, the sixfold fermions have not been well investigated in spin-free systems both theoretically and experimentally due to the lack of ideal target materials. Specifically, spin-orbit coupling (SOC) always breaks the sixfold fermions in electronic systems; moreover, these fermions lie normally far from the Fermi level [22].

Topological bosons [23–28] also show elementary excitations in condensed matter systems. Additionally, topological phonons [29–40] exist in crystalline solids, as the basic emergent boson of the crystalline lattice, due to the crystal symmetry constraints. Parallel to electronic systems, twofold degenerate Weyl point [31–33,36,37], triple nodal point [28,29], and fourfold degenerate Dirac point [30] phonons have already been predicted in phonon systems. Furthermore, double Weyl point phonons have been experimentally verified

*These authors contributed equally to this work.
†Corresponding author: zzy@mail.buct.edu.cn
‡Corresponding author: xiaotianwang@swu.edu.cn
§Corresponding author: zhangg@ihpc.a-star.edu.sg

in FeSi type systems [33]. However, the sixfold degenerate nodal-point phonons have been rarely reported. Moreover, compared to nodal-point phonons with two-, three-, and fourfold degenerate, the sixfold excitations have attracted considerable interest owing to the presence of the maximum degeneracy in bosonic systems [3,22].

In this study we screened all 230 SGs, and found the sixfold degenerate nodal-point phonons can appear in five candidate groups (with SG Nos. 218, 220, 222, 223, and 230). Such sixfold degenerate—the maximal degenerate [22]—nodal-point phonons in phonon systems do not have the restriction of the Pauli exclusion principle and without SOC effect [37]. Guided by the symmetry analysis, we proposed that realistic materials C_3N_4, Sc_4C_3, and Y_4Sb_3 with SG No. 220, Li_7VN_4 with SG No. 218, K_8Si_{46} with SG No. 223, $Ca_3Ge_3O_{12}Sc_2$ with SG No. 230, and a theoretically assumed cagelike nanoporous polymorphs (named as KFI phase) composed of spheroidal cages $(ZnO)_{24}$ with SG No. 222, are candidates with sixfold degenerate nodal-point phonons. As examples, the phonon surface states of C_3N_4, Sc_4C_3, Y_4Sb_3, and K_8Si_{46} materials were studied in detail based on the first-principles calculations. We constructed effective models around the sixfold degenerate points, proposed a series of existing topological materials with sixfold degenerate excitations, and paved a way to search for sixfold degenerate phonons in the future.

II. $k \cdot p$ MODELS AROUND THE SIXFOLD DEGENERATE POINT PHONONS

After screening all 230 SGs, we find that the sixfold degenerate nodal-point phonons can appear in the spinless phonon systems with SG Nos. 218, 220, 222, 223, and 230. The followings are the detailed $k\cdot p$ models around the sixfold degenerate point phonons in five candidate groups.

Nos. 218 and 220 SGs. Consider the $R(\frac{1}{2},\frac{1}{2},\frac{1}{2})$ and $H(\frac{1}{2},-\frac{1}{2},\frac{1}{2})$ point in Nos. 218 and 220 SGs. The little group of R or H share the same rotation part. By calculating the co-representation of R (H) point in No. 218 (220) SG, there exist two different three-dimensional irreducible representation "stick" together by time-reversal symmetry [41]. A set of generators and matrix representation for the sixfold co-representation can be chosen as follows:

$$C_{2z} = \sigma_0 \otimes \begin{pmatrix} -1 & 0 & 0 \\ 0 & 1 & 0 \\ 0 & 0 & 1 \end{pmatrix}, \quad C_{2x} = \sigma_0 \otimes \begin{pmatrix} 1 & 0 & 0 \\ 0 & 1 & 0 \\ 0 & 0 & -1 \end{pmatrix},$$

$$\sigma_{da} = \sigma_3 \otimes \begin{pmatrix} i & 0 & 0 \\ 0 & 0 & i \\ 0 & i & 0 \end{pmatrix}, \quad C_{31}^{+} = \sigma_0 \otimes \begin{pmatrix} 0 & 1 & 0 \\ 0 & 0 & -1 \\ -1 & 0 & 0 \end{pmatrix},$$

$$\mathcal{T} = \sigma_1 \otimes \begin{pmatrix} 1 & 0 & 0 \\ 0 & 1 & 0 \\ 0 & 0 & 1 \end{pmatrix},$$

where σ_i are Pauli matrices. Then the effective Hamiltonian for No. 218 (220) SG at R (H) constrained by these symmetries can be shown as follows:

$$H_{\mathrm{SP}}^{218,220} = \begin{pmatrix} 0 & -ck_x & ck_y & 0 & -\alpha k_x & -\alpha k_y \\ -ck_x & 0 & ck_z & \alpha k_x & 0 & \alpha k_z \\ ck_y & ck_z & 0 & \alpha k_y & -\alpha k_z & 0 \\ 0 & \alpha k_x & \alpha k_y & 0 & ck_x & -ck_y \\ -\alpha k_x & 0 & -\alpha k_z & ck_x & 0 & -ck_z \\ -\alpha k_y & \alpha k_z & 0 & -ck_y & -ck_z & 0 \end{pmatrix}, \tag{1}$$

where c is a real parameter and α is a complex parameter.

Nos. 222 and 223 SGs. In No. 222 (223) SG, there exist a six-dimensional irreducible representation at R point. A set of generators and matrix representation for the sixfold irreducible representation can be chosen as follows:

$$C_{2z} = \begin{pmatrix} -1 & 0 & 0 & 0 & 0 & 0 \\ 0 & -1 & 0 & 0 & 0 & 0 \\ 0 & 0 & -1 & 0 & 0 & 0 \\ 0 & 0 & 0 & 1 & 0 & 0 \\ 0 & 0 & 0 & 0 & -1 & 0 \\ 0 & 0 & 0 & 0 & 0 & 1 \end{pmatrix},$$

$$C_{2x} = \begin{pmatrix} 1 & 0 & 0 & 0 & 0 & 0 \\ 0 & 1 & 0 & 0 & 0 & 0 \\ 0 & 0 & -1 & 0 & 0 & 0 \\ 0 & 0 & 0 & -1 & 0 & 0 \\ 0 & 0 & 0 & 0 & -1 & 0 \\ 0 & 0 & 0 & 0 & 0 & -1 \end{pmatrix},$$

$$C_{2a} = \begin{pmatrix} 0 & 0 & -1 & 0 & 0 & 0 \\ 0 & 0 & 0 & 0 & 1 & 0 \\ -1 & 0 & 0 & 0 & 0 & 0 \\ 0 & 0 & 0 & -1 & 0 & 0 \\ 0 & 1 & 0 & 0 & 0 & 0 \\ 0 & 0 & 0 & 0 & 0 & 1 \end{pmatrix},$$

$$C_{31}^{+} = \begin{pmatrix} 0 & 0 & 0 & -1 & 0 & 0 \\ 0 & 0 & 0 & 0 & 0 & 1 \\ -1 & 0 & 0 & 0 & 0 & 0 \\ 0 & 0 & 1 & 0 & 0 & 0 \\ 0 & -1 & 0 & 0 & 0 & 0 \\ 0 & 0 & 0 & 0 & -1 & 0 \end{pmatrix}, \quad I = \begin{pmatrix} 0 & 1 & 0 & 0 & 0 & 0 \\ 1 & 0 & 0 & 0 & 0 & 0 \\ 0 & 0 & 0 & 0 & 1 & 0 \\ 0 & 0 & 0 & 0 & 0 & -1 \\ 0 & 0 & 1 & 0 & 0 & 0 \\ 0 & 0 & 0 & -1 & 0 & 0 \end{pmatrix},$$

$\mathcal{T} = E$ (E is identity matrix). Hence the effective Hamiltonian for No. 222 (223) SG at R can be written by

$$H_{\mathrm{SP}}^{222,223} = \begin{pmatrix} 0 & 0 & -ic_1k_z & ic_1k_y & ic_2k_z & -ic_2k_y \\ 0 & 0 & -ic_2k_z & -ic_2k_y & ic_1k_z & ic_1k_y \\ ic_1k_z & ic_2k_z & 0 & ic_1k_x & 0 & ic_2k_x \\ -ic_1k_y & ic_2k_y & -ic_1k_x & 0 & -ic_2k_x & 0 \\ -ic_2k_z & -ic_1k_z & 0 & ic_2k_x & 0 & ic_1k_x \\ ic_2k_y & -ic_1k_y & -ic_2k_x & 0 & -ic_1k_x & 0 \end{pmatrix}, \tag{2}$$

where c_i are real parameters.

No. 230 SG. Similar to Nos. 222 and 223 SGs, there also exist a six-dimensional irreducible representation at H point in No. 230 SG. However, the matrix representation of little group at H in No. 230 SG is different from R point in No. 222 (223) SG. This is because the Herring little group for H in No. 230 SG is not isomorphic to the Herring little group for R point in No. 222 (223) SG [42]. A set of generators and matrix representation for the sixfold irreducible representation can be chosen to be

$$C_{2z} = \sigma_0 \otimes \begin{pmatrix} 1 & 0 & 0 \\ 0 & -1 & 0 \\ 0 & 0 & 1 \end{pmatrix}, \quad C_{2x} = \sigma_0 \otimes \begin{pmatrix} -1 & 0 & 0 \\ 0 & 1 & 0 \\ 0 & 0 & 1 \end{pmatrix},$$

$$C_{2a} = i\sigma_2 \otimes \begin{pmatrix} 0 & 0 & i \\ 0 & -i & 0 \\ i & 0 & 0 \end{pmatrix}, \quad C_{31}^{+} = \sigma_0 \otimes \begin{pmatrix} 0 & -1 & 0 \\ 0 & 0 & -1 \\ 1 & 0 & 0 \end{pmatrix},$$

$$I = \sigma_1 \otimes \begin{pmatrix} 1 & 0 & 0 \\ 0 & 1 & 0 \\ 0 & 0 & 1 \end{pmatrix}, \quad \mathcal{T} = \sigma_1 \otimes \begin{pmatrix} 1 & 0 & 0 \\ 0 & 1 & 0 \\ 0 & 0 & 1 \end{pmatrix},$$

the effective Hamiltonian can be written by

$$H_{\mathrm{SP}}^{230} = \begin{pmatrix} 0 & c_1k_y & -c_1k_z & 0 & c_2k_y & c_2k_z \\ c_1k_y & 0 & c_1k_x & -c_2k_y & 0 & c_2k_x \\ -c_1k_z & c_1k_x & 0 & -c_2k_z & -c_2k_x & 0 \\ 0 & -c_2k_y & -c_2k_z & 0 & -c_1k_y & c_1k_z \\ c_2k_y & 0 & -c_2k_x & -c_1k_y & 0 & -c_1k_x \\ c_2k_z & c_2k_x & 0 & c_1k_z & -c_1k_x & 0 \end{pmatrix}, \tag{3}$$

where c_i are real parameters.

TABLE I. Experimental and theoretical lattice constants of C_3N_4, Sc_4C_3, and Y_4Sb_3.

Materials	Experimental lattice constants ($a/b/c$)	Theoretical lattice constants ($a/b/c$)
C_3N_4	5.360 Å [48]	5.447 Å
Sc_4C_3	7.206 Å [50]	7.227 Å
Y_4Sb_3	9.139 Å [52]	9.216 Å

Note that, in Nos. 218 and 220 SGs, the sixfold nodal point is strongly depending on the $\mathcal{T}$, i.e., when the $\mathcal{T}$ is broken, the sixfold nodal point may split into two threefold nodal points. However, in Nos. 222, 223, and 230 SGs, the $\mathcal{T}$ is not necessary to protect the sixfold nodal point.

III. CALCULATION METHODS

We used density functional theory [43] to work with the ground states of target materials in Secs. III and IV. Furthermore, we employed GGA-PBE [44] formalism for the exchange-correlation functional. The projector augmented-wave [45] method was used for the interactions between ions and valence electrons. The energy cutoff was set to 500 eV. Moreover, for C_3N_4, Sc_4C_3, and Y_4Sb_3 with SG No. 220, a Γ-centered k mesh of $9 \times 9 \times 9$ was used for Brillouin zone (BZ) sampling, however, for materials with SG Nos. 218, 222, 223, and 230, a Γ-centered k mesh of $3 \times 3 \times 3$ was used for Brillouin zone (BZ) sampling. We performed a dynamic calculation of lattice to obtain the phonon dispersion at ground states in the PHONOPY package [46] using density functional perturbation theory [47] to investigate the topological phonon signatures of the proposed materials. For C_3N_4, Sc_4C_3, and Y_4Sb_3 with SG No. 220, we built $2 \times 2 \times 2$ supercells to obtain the phonon dispersion. However, for the other materials with SG Nos. 218, 222, 223, 230, and larger unit cells, we used the cubic unit cells directly to calculate the phonon dispersion due to these systems contain more than 50 atoms. As examples, we determined (110) phonon surface states of the C_3N_4, Sc_4C_3, and Y_4Sb_3 materials and the (100) phonon surface states of the K_8Si_{48} by constructing a Wannier tight-binding Hamiltonian of phonons [46].

IV. SIXFOLD DEGENERATE NODAL-POINT PHONONS IN MATERIALS WITH SPACE GROUP NUMBER 220

In this section we come to focus on three existing materials C_3N_4, Sc_4C_3, and Y_4Sb_3 with No. 220 SG. Zhang *et al.* [48] fabricated C-N thin films by plasma-enhanced chemical vapor deposition. They indicated that C-N thin films contain $I\bar{4}3d$ type C_3N_4, which is in a good agreement with the theoretical prediction by Teter and Hemley [49]. Krikorian *et al.* [50] proposed Sc_4C_3 as a cubic system with $I\bar{4}3d$ type structure by arc-melt preparations. Schmidt and Macmasters [51] experimentally predicted a phase diagram of the Y-Sb system. They showed that Y_4Sb_3 results from peritectic reactions at 2120 °C. The experimental and the theoretical lattice constants are shown in Table I. We note that the lattice constants derived in this work are in good agreements with those derived in experiments. Figure 1 shows the crystal structures of these three materials. The atomic positions of these materials are as follows: (1) C_3N_4 with C 12a (0.875, 0.0, 0.25) and N 16c (0.2812, 0.2812, 0.2812); (2) Sc_4C_3 with Sc 16c (0.0476, 0.0496, 0.0496) and C 12a (0.375, 0.0, 0.25); (3) Y_4Sb_3 with Y 16c (0.074, 0.074, 0.074) and Sb 12b (0.375, 0.0, 0.25).

Figures 2(b)–2(d) show the phonon dispersion of C_3N_4, Sc_4C_3, and Y_4Sb_3 materials along the high-symmetry lines as listed in Fig. 2(a), respectively. All the phonon frequencies show that the selected materials with No. 220 SG are dynamically stable. Furthermore, we focus on the regions of phonon frequencies with a purple background in Figs. 2(b)–2(d). The enlarged phonon frequencies of these purple regions are shown in Figs. 3(b)–3(d), respectively. In the frequency regions of 36–37 THz, 15.52–15.62 THz, and 4.97–5.00 THz of C_3N_4, Sc_4C_3, and Y_4Sb_3, respectively, doubly degenerate phonon bands merged at the H point along the N-H direction to form a sixfold degenerate phonon band crossing with linear dispersion. The schematic diagram of the sixfold degenerate nodal-point phonons state is shown in Fig. 3(a). We note that the sixfold degenerate nodal-point phonons show maximum degeneracy in phonon systems; moreover, such sixfold excitations in spin-free systems have not been studied well [2]. This study proves that realistic materials can host sixfold degenerate nodal-point states in their phonon dispersions and show a new direction for follow-up works related to the multifold degenerate excitations in topological phonons.

The local density of states (LDOS) of phonons of these three materials were obtained using the iterative Green's function method [52]. The LDOS of C_3N_4, Sc_4C_3, and Y_4Sb_3 on the semi-infinite (110) plane [see Fig. 4(a)] are shown in Figs. 4(b)–4(d), respectively. The behaviors of the sixfold degenerate nodal points of C_3N_4, Sc_4C_3, and Y_4Sb_3 are highlighted with white circles at ∼36.576, ∼15.567, and ∼4.984 THz, respectively. Two obvious phonon surface states (marked by the white arrows) from the sixfold degenerate

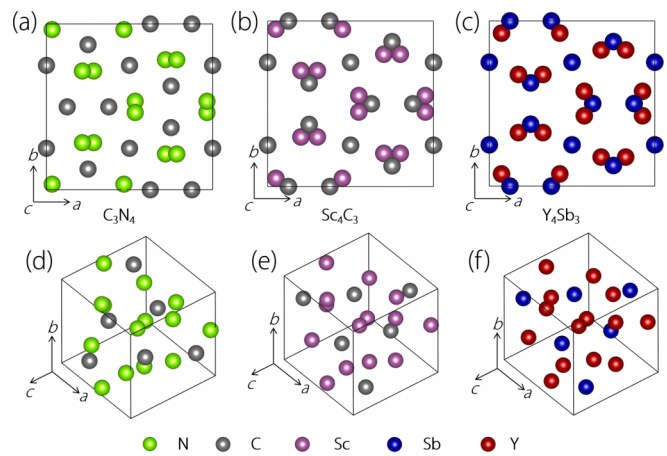

FIG. 1. Unit cells (a)–(c) and primitive cells (d) and (e) of C_3N_4, Sc_4C_3, and Y_4Sb_3 with $I\bar{4}3d$ type structure, respectively.

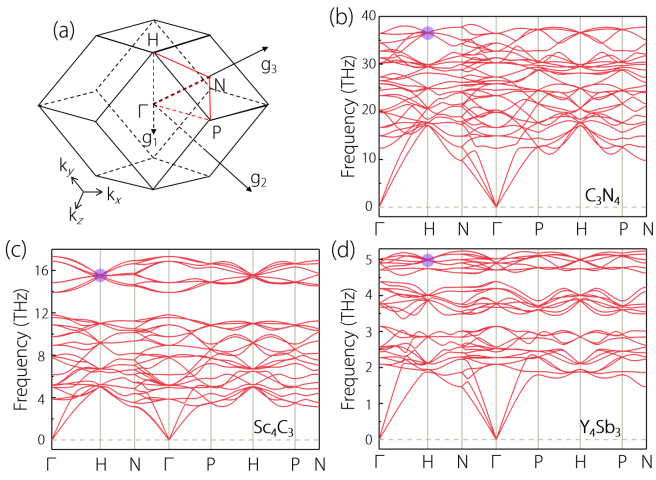

FIG. 2. (a) Three-dimensional coordinate system of the BZ and some high symmetry points. (b)–(d) Phonon dispersions of C_3N_4, Sc_4C_3, and Y_4Sb_3, respectively. Purple circles in (b)–(d) mark the topological signatures of our interest.

nodal points are visible, which would benefit the experimental observation in future experiments.

V. SIXFOLD DEGENERATE NODAL-POINT PHONONS IN MATERIALS WITH SPACE GROUP NUMBERS 218, 222, 223, 230

In this section some materials with SG Nos. 218, 222, 223, 230, and large cubic unit cells are reported to be the hosts to exhibit sixfold degenerate nodal-point phonons at their high-symmetry points R or H (see Sec. II).

Li_7VN_4 with $P\bar{4}3n$ (SG No. 218) was selected as an example to prove the sixfold nodal-point phonons can appear at the R point in three-dimensional (3D) BZ of phononic systems with No. 218 SG. The Li-V-N systems were studied by Niewa

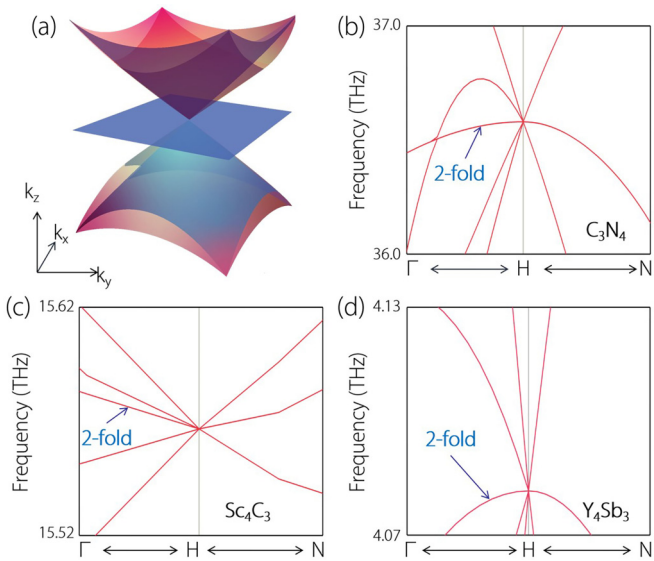

FIG. 3. (a) The schematic diagram of a state of sixfold degenerate nodal point phonons. (b)–(d) The enlarged phonon frequencies of Figs. 2(b)–2(d) with sixfold degenerate nodal-point phonons.

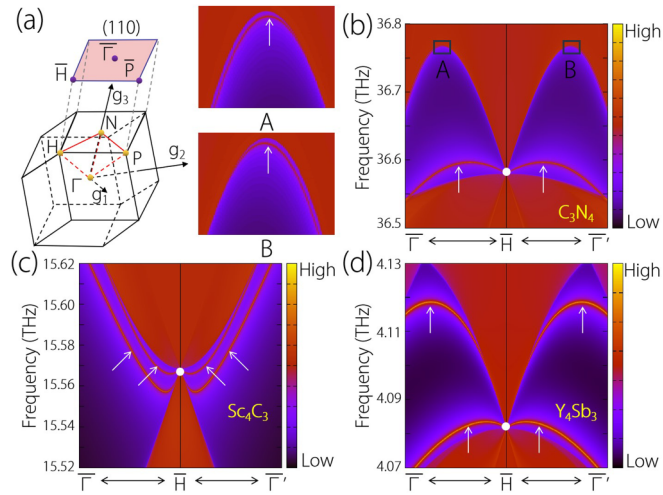

FIG. 4. (a) The bulk BZ and the surface BZ along the (110) direction of target materials. (b)–(d) The phonon surface states of C_3N_4, Sc_4C_3, and Y_4Sb_3 along the $\bar{\Gamma}$-$\bar{H}$-$\bar{\Gamma}'$ of the (110) surface BZ, respectively. The white circles denote the bulk sixfold degenerate nodal-point states, and the red lines marked by white arrows represent the phonon surface states.

et al. [53] via x-ray and neutron powder diffraction in 2002. The γ -type Li_7VN_4 (with No. 218 SG) can form from Li_3N and VN at 920 K (30 h) or 1020 K (10 h) in N_2 atmosphere. The crystal structure of γ -type Li_7VN_4 is shown in Fig. 5(a), which contains 96 atoms (8 V, 32 N, and 56 Li atoms). The obtained lattice constants via DFT are $a = b = c = 9.604$ Å, which are in good agreements with the experimental values ($a = b = c = 9.609$ Å) [53]. Then, based on density functional perturbation theory method, we calculate the phonon dispersion of the Li_7VN_4 with cubic unit cell [as exhibited in Fig. 5(a)] along the high-symmetry lines Γ-*X*-*M*-Γ-*R*-*X*-*R*-*M* [as listed in Fig. 5(b)]. The results are shown in Figs. 5(c) and 5(d). Obviously one can see the Li_7VN_4 is dynamical stable and the sixfold nodal-point phonons occurring at the R point, which is consistent with the symmetry analysis in Sec. II.

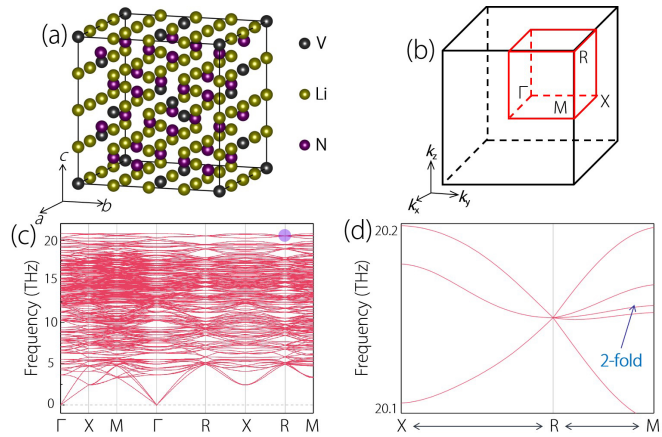

FIG. 5. (a) Crystal structure of γ -type Li_7VN_4 with No. 218 SG. (b) The bulk BZ and some high symmetry points. (c) Calculated phonon dispersion for $P\bar{4}3n$ type Li_7VN_4. (d) Enlarged phonon frequencies of the purple area in (c).

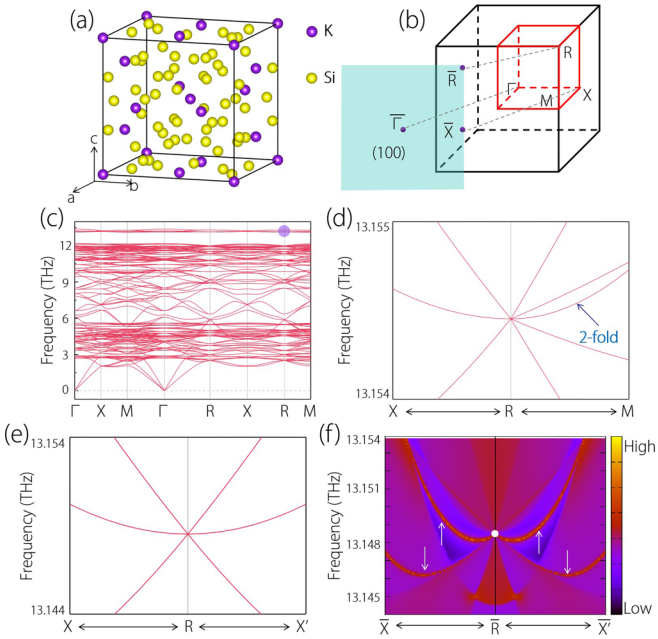

FIG. 6. (a) Crystal structure of K_8Si_{46} with SG No. 223. (b) The bulk BZ and the surface BZ along the (100) direction. (c) Calculated phonon dispersion for $Pm\bar{3}n$ type K_8Si_{46}. (d) Enlarged phonon frequencies of the purple area in Fig. 6(c). (e) The phonon frequencies of K_8Si_{46} bulk along X-R-X' paths. (f) The phonon surface states of K_8Si_{46} along the $\bar{X}$-$\bar{R}$-$\bar{X}'$ of the (100) surface BZ, respectively. The white circle denote the bulk sixfold degenerate nodal point state, and the red lines marked by white arrows represent the phonon surface states.

K_8Si_{46} with $Pm\bar{3}n$ type structure (SG No. 223) has been proved to be an existing material before [54] and K_8Si_{46} sample can be prepared by treating stoichiometric mixtures of the elements (K and Si) at 666 °C for 24 h. The crystal structure of K_8Si_{46} is shown in Fig. 6(a) and the calculated lattice constants ($a = b = c = 10.342$ Å) are close to the experimental values ($a = b = c = 10.260$ Å) [54]. The cubic unit cell of $Pm\bar{3}n$ type K_8Si_{46} includes 54 atoms, i.e., 8 K and 46 Si atoms. The phonon dispersion of K_8Si_{46} with cubic unit cell are calculated along the Γ-X-M-Γ-R-X-R-M paths [see Fig. 6(b)]. We exhibited the results in Figs. 6(c) and 6(d). It can be seen that no acoustic-optical branch gap appears in the phonon spectra and K_8Si_{46} is dynamically stable due to the absence of imaginary frequencies. Figure 6(d) shows the enlarged phonon frequencies of the purple region in Fig. 6(c) along X-R-M paths. Along X-R paths, one can see three twofold degenerate phonon bands merge at R point to form a sixfold degenerate phonon band crossing with linear dispersion [see Fig. 6(d)]. We would like to point out that such sixfold degenerate nodal points in phonon systems with No. 223 SG belong to symmetry-enforced nodal points (refer to Sec. II). The LDOS of phonons of K_8Si_{46} along the $\bar{X}$-$\bar{R}$-$\bar{X}'$ of the (100) surface BZ are shown in Fig. 6(f). As a reference, the phonon frequencies of K_8Si_{46} bulk along X-R-X' paths are exhibited in Fig. 6(e). One indeed observes two phonon surface states, as highlighted by white arrows.

Thanks to the symmetry-enforced behaviors, we can search for materials with sixfold degenerate nodal-point phonons according to the symmetry analysis as given in Sec. II. However, for No. 222 SG, material realization is still a big challenge for us due to lack of ideal material candidates. We failed to identify a realistic material with SG No. 222 as a host of sixfold degenerate nodal-point phonons after making significant efforts. Fortunately, Tuoc *et al.* [55] theoretically proposed a cagelike nanoporous polymorphs (named as KFI phase) composed of spheroidal cages $(ZnO)_{24}$ as a building block in high symmetrical cubic lattice frameworks. The crystal structure of the proposed KFI nanoporous phase is exhibited in Fig. 7(a). This cubic unit cell contains 96 atoms (48 Zn and 48 O atoms). The Zn and O occupy the 48i (0.08, 0.20,0.32) and O with 48i (0.58, 0.70, 0.82) Wyckoff positions, respectively. Based on the selected high-symmetry paths in Fig. 7(b), the calculated phonon dispersion of the cubic unit cell is shown in Figs. 7(c) and 7(d). Consistent with our symmetry analysis in Sec. II, the sixfold degenerate nodal-point phonons appear at R point.

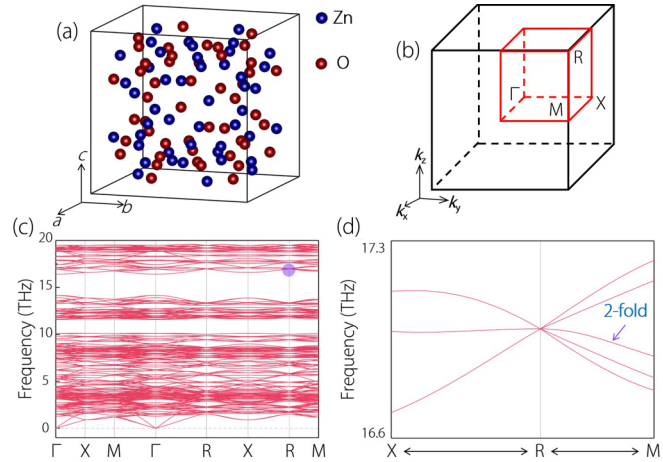

FIG. 7. (a) Crystal structure of 3D ZnO cagelike nanoporous phase (named as KFI phase) with SG No. 222. The cubic unit cell of the KFI phase has 96 atoms. (b) The bulk BZ and some high symmetry points. (c) Calculated phonon dispersion for KFI nanoporous phase. (d) Enlarged phonon frequencies of the purple area in (c).

$Ca_3Ge_3O_{12}Sc_2$ crystal was prepared via the flux growth technique by Mill [56]. The unit cell of $Ca_3Ge_3O_{12}Sc_2$ with $Ia\bar{3}d$ type structure (with SG No. 230) is shown in Fig. 8(a). This system is cubic with calculated lattice constants $a = b = c = 12.645$ Å, includes eight formula units, and contains 80 atoms, i.e., 12 Ga, 8 Sc, 12 Ge, and 48 O atoms. The obtained lattice constants are are close to the experimental values ($a = b = c = 12.512$ Å) [56]. The cubic unit cell is chosen to calculate the phonon dispersion along Γ-H-N-Γ-P-H-P-N paths [see Fig. 8(b)]. According to the results exhibited in Figs. 8(c) and 8(d), a sixfold degenerate nodal point at ∼15 THz can be clearly observed at H point.

VI. REMARKS AND CONCLUSIONS

In summary, by checking the symmetries of 230 SGs, we found the sixfold degenerate nodal-point phonons can appear at the high-symmetry points (R or H) of the SGs (with Nos. 218, 220, 222, 223, and 230). The proposed sixfold degenerate nodal point in spinless phonon systems

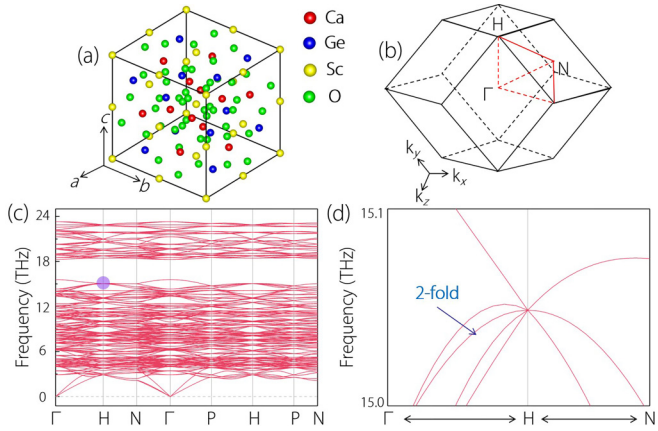

FIG. 8. (a) Crystal structure of $Ca_3Ge_3O_{12}Sc_2$ with SG No. 230. (b) The bulk BZ and some high symmetry points. (c) Calculated phonon dispersion for $Ia\bar{3}d$ type $Ca_3Ge_3O_{12}Sc_2$. (d) Enlarged phonon frequencies of the purple area in (c).

belongs to a symmetry-enforced point, and we can search for material candidates with sixfold degenerate nodal-point phonons among existing materials based on the symmetry conditions as discussed in Sec. II. As examples, we proposed that some realistic materials, including C_3N_4, Sc_4C_3, Y_4Sb_3 (with SG No. 220), Li_7VN_4 (with SG No. 218), K_8Si_{46} (with SG No. 223), and $Ca_3Ge_3O_{12}Sc_2$ (with SG No. 230) are candidates with sixfold degenerate nodal-point phonons. Also, we exhibited that a theoretically assumed KFI phase, composed of spheroidal cages $(ZnO)_{24}$, (with SG No. 222), is a candidate to study the sixfold degenerate nodal-point phonon states. Moreover, we selected C_3N_4, Sc_4C_3, Y_4Sb_3, and K_8Si_{46} materials as targets to study the phonon surface spectrum. We found two clear phonon surface states arising from these multiple degenerate nodal points. We would like to point out that phonon systems with the SG Nos. 218, 220, 222, 223, and 230 are ideal targets to study unconventional sixfold quasiparticles because they do not face restrictions posed by SOC and Pauli exclusion principle.

The following are some remarks: (1) We note that the materials hosting sixfold (the maximum-fold) degenerate nodal point phonons have been rarely reported [2,22]. (2) In many electronic systems with sixfold degenerate fermions, the sixfold degenerate band crossings do not sit at (or around) the Fermi level. However, the sixfold degenerate phononic systems do not follow the limitation set by the Pauli exclusion principle. Therefore, the sixfold degenerate nodal point phonons can be found in a large range of phonon frequencies. (3) The spinless sixfold degenerate nodal point states are usually gapped in electronic systems due to the effect of SOC. Hence, it is challenging to host ideal sixfold degenerate fermions in spinless electronic systems. The phonon systems, unlike electronic systems, with negligible SOC effect can be seen as a feasible platform to investigate the ideal spinless sixfold excitations. (4) Fortunately, two surface states in the (110) plane for C_3N_4, Sc_4C_3, Y_4Sb_3 materials and the (100) plane for K_8Si_{46} material are visible, which is good for experimental observations.

ACKNOWLEDGMENTS

Z.Z. acknowledges the support by China Postdoctoral Science Foundation (Grant No. 2020M670106) and the National Natural Science Foundation of China (Grant No. 12004028). X.W. is grateful for the support from the National Natural Science Foundation of China (No. 51801163) and the Natural Science Foundation of Chongqing (No. cstc2018jcyjA0765). X.W. thanks Prof. Zhi-Ming Yu for his help regarding this paper.

[1] P. B. Pal, Am. J. Phys. **79**, 485 (2011).
[2] H. Gao, J. W. Venderbos, Y. Kim, and A. M. Rappe, Annu. Rev. Mater. Res. **49**, 153 (2019).
[3] Z. M. Yu, Z. Y. Zhang, G. B. Liu, W. K. Wu, X. P. Li, R. W. Zhang, S. Y. A Yang, and Y. G. Yao, arXiv:2102.01517v3.
[4] Z. Zhu, G. W. Winkler, Q. S. Wu, J. Li, and A. A. Soluyanov, Phys. Rev. X **6**, 031003 (2016).
[5] B. Bradlyn, J. Cano, Z. Wang, M. G. Vergniory, C. Felser, R. J. Cava, and B. A. Bernevig, Science **353**, aaf5037 (2016).
[6] J. L. Manes, Phys. Rev. B **85**, 155118 (2012).
[7] H. Weng, C. Fang, Z. Fang, and X. Dai, Phys. Rev. B **93**, 241202(R) (2016).
[8] G. Chang, S. Y. Xu, S. M. Huang, D. S. Sanchez, C. H. Hsu, G. Bian *et al.*, Sci. Rep. **7**, 1 (2017).
[9] H. Yang, J. Yu, S. S. P. Parkin, C. Felser, C.-X. Liu, and B. Yan, Phys. Rev. Lett. **119**, 136401 (2017).
[10] W. Gao, X. Zhu, F. Zheng, M. Wu, J. Zhang, C. Xi *et al.*, Nat. Commun. **9**, 1 (2018).
[11] B. Q. Lv, Z. L. Feng, Q. N. Xu, X. Gao, J. Z. Ma, L. Y. Kong *et al.*, Nature (London) **546**, 627 (2017).
[12] J. Z. Ma, J. B. He, Y. F. Xu, B. Q. Lv, D. Chen, and W. L. Zhu, Nat. Phys. **14**, 349 (2018).
[13] B. J. Wieder, Y. Kim, A. M. Rappe, and C. L. Kane, Phys. Rev. Lett. **116**, 186402 (2016).
[14] X. Zhang, Q. Gu, H. Sun, T. Luo, Y. Liu, Y. Chen, Z. Shao, Z. Zhang, S. Li, Y. Sun, Y. Li, X. Li, S. Xue, J. Ge, Y. Xing, R. Comin, Z. Zhu, P. Gao, B. Yan, J. Feng, M. Pan, and J. Wang, Phys. Rev. B **102**, 035125 (2020).
[15] N. B. Schröter, D. Pei, M. G. Vergniory, Y. Sun, K. Manna, F. De Juan *et al.*, Nat. Phys. **15**, 759 (2019).
[16] C. K. Barman, C. Mondal, S. Pujari, B. Pathak, and A. Alam, Phys. Rev. B **102**, 155147 (2020).
[17] M. Nishiyama, Y. Inada, and G. Q. Zheng, Phys. Rev. Lett. **98**, 047002 (2007).
[18] K. W. Lee and W. E. Pickett, Phys. Rev. B **72**, 174505 (2005).
[19] N. Kumar, M. Yao, J. Nayak, M. G. Vergniory, J. Bannies, Z. Wang, N. B. M. Schröter, V. N. Strocov, L. Möchler, W. Shi, E. D. L. Rienks, J. L. Maões, C. Shekhar, S. S. P. Parkin, J. Fink, G. H. Fecher, Y. Sun, B. A. Bernevig, and C. Felser, Adv. Mater. **32**, 1906046 (2020).
[20] Z. P. Sun, C. Q. Hua, X. L. Liu, Z. T. Liu, M. Ye, S. Qiao, Z. H. Liu, J. S. Liu, Y. F. Guo, Y. H. Lu, and D. W. Shen, Phys. Rev. B **101**, 155114 (2020).

[21] X. Yáng, T. A. Cochran, R. Chapai, D. Tristant, J.-X. Yin, I. Belopolski, Z. Chéng, D. Multer, S. S. Zhang, N. Shumiya, M. Litskevich, Y. Jiang, G. Chang, Q. Zhang, I. Vekhter, W. A. Shelton, R. Jin, S.-Y. Xu, and M. Z. Hasan, Phys. Rev. B, **101**, 201105(R) (2020).
[22] S. Nie, B. A. Bernevig, and Z. Wang, Phys. Rev. Res. **3**, L012028 (2021).
[23] L. Jin, Y. Liu, X. Zhang, X. Dai, and G. Liu, Phys. Rev. B **104**, 045111 (2021).
[24] Y. Jin, R. Wang, and H. Xu, Nano Lett. **18**, 7755 (2018).
[25] S. B. Zhang and J. Zhou, Phys. Rev. B **101**, 085202 (2020).
[26] Q. Xie, J. Li, S. Ullah, R. Li, L. Wang, D. Li, Y. Li, S. Yunoki, and X. Q. Chen, Phys. Rev. B **99**, 174306 (2019).
[27] Y. Liu, Y. Xu, S. C. Zhang, and W. Duan, Phys. Rev. B **96**, 064106 (2017).
[28] O. Stenull, C. L. Kane, and T. C. Lubensky, Phys. Rev. Lett. **117**, 068001 (2016).
[29] S. Singh, Q. S. Wu, C. Yue, A. H. Romero, and A. A. Soluyanov, Phys. Rev. Mater. **2**, 114204 (2018).
[30] J. Li, L. Wang, J. Liu, R. Li, Z. Zhang, and X.-Q. Chen, Phys. Rev. B **101**, 081403(R) (2020).
[31] J. Liu, W. Hou, E. Wang, S. Zhang, J.-T. Sun, and S. Meng, Phys. Rev. B **100**, 081204(R) (2019).
[32] T. Zhang, Z. Song, A. Alexandradinata, H. Weng, C. Fang, L. Lu, and Z. Fang, Phys. Rev. Lett. **120**, 016401 (2018).
[33] H. Miao, T. T. Zhang, L. Wang, D. Meyers, A. H. Said, Y. L. Wang, Y. G. Shi, H. M. Weng, Z. Fang, and M. P. M. Dean, Phys. Rev. Lett. **121**, 035302 (2018).
[34] Y. J. Jin, Z. J. Chen, B. W. Xia, Y. J. Zhao, R. Wang, and H. Xu, Phys. Rev. B **98**, 220103(R) (2018).
[35] J. Li, J. Liu, S. A. Baronett, M. Liu, L. Wang, R. Li, Y. Chen, D. Li, Q. Zhu, and X. Chen, Nat. Commun. **12**, 1204 (2020).
[36] B. W. Xia, R. Wang, Z. J. Chen, Y. J. Zhao, and H. Xu, Phys. Rev. Lett. **123**, 065501 (2019).
[37] R. Wang, B. W. Xia, Z. J. Chen, B. B. Zheng, Y. J. Zhao, and H. Xu, Phys. Rev. Lett. **124**, 105303 (2020).
[38] Q. Liu, H. Fu, G. Xu, R. Yu, and R. J. Wu, J. Phys. Chem. Lett. **10**, 4045 (2019).
[39] J. Li, Q. Xie, J. Liu, R. Li, M. Liu, L. Wang, D. Li, Y. Li, and X.-Q. Chen, Phys. Rev. B **101**, 024301 (2020).
[40] T. T. Zhang, H. Miao, Q. Wang, J. Q. Lin, Y. Cao, G. Fabbris, A. H. Said, X. Liu, H. C. Lei, Z. Fang, H. M. Weng, and M. P. M. Dean, Phys. Rev. Lett. **123**, 245302 (2019).
[41] G.-B. Liu, M. Chu, Z. Zhang, Z.-M. Yu, and Y. Yao, Comput. Phys. Commun. **265**, 107993 (2021).
[42] C. Bradley and A. Cracknell, *The Mathematical Theory of Symmetry in Solids: Representation Theory for Point Groups and Space Groups* (Oxford University Press, New York, 1972).
[43] E. K. Gross and R. M. Dreizler (Eds.), *Density Functional Theory* (Springer Science and Business Media, New York, 2013), Vol. 337.
[44] J. P. Perdew, K. Burke, and M. Ernzerhof, Phys. Rev. Lett. **77**, 3865 (1996).
[45] P. E. Blöchl, Phys. Rev. B **50**, 17953 (1994).
[46] A. Togo and I. Tanaka, Scr. Mater. **108**, 1 (2015).
[47] S. Baroni, S. De Gironcoli, A. Dal Corso, and P. Giannozzi, Rev. Mod. Phys. **73**, 515 (2001).
[48] Z. Zhang, H. Guo, G. Zhong, F. Yu, Q. Xiong, and X. Fan, Thin Solid Films **346**, 96 (1999).
[49] D. M. Teter and R. J. Hemley, Science **271**, 53 (1996).
[50] N. H. Krikorian, A. L. Bowman, M. C. Krupka, and G. P. Arnold, High Temp. Sci. **1**, 360 (1969).
[51] F. A. Schmidt and O. D. McMasters, J. Less-Common Met. **21**, 415 (1970).
[52] Q. Wu, S. Zhang, H. F. Song, M. Troyer, and A. A. Soluyanov, Comput. Phys. Commun. **224**, 405 (2018).
[53] R. Niewa, D. Zherebtsov, and Z. Hu, Inorg. Chem. **42**, 2538 (2003).
[54] G. K. Ramachandran, P. F. McMillan, J. Dong, and O. F. Sankey, J. Solid State Chem. **154**, 626 (2000).
[55] V. N. Tuoc, T. D. Huan, and N. T. Thao, Mater. Today Commun. **24**, 101152 (2020).
[56] B. V. Mill, Kristallogr. **19**, 1057 (1974).